Journal of Environmental Radioactivity 161 (2016) 11–21

Contents lists available at ScienceDirect

Journal of Environmental Radioactivity

journal homepage: www.elsevier.com/locate/jenvrad

Input and output budgets of radiocesium concerning the forest floor in the mountain forest of Fukushima released from the TEPCO's Fukushima Dai-ichi nuclear power plant accident

Tadafumi Niizato*, Hironobu Abe, Katsuaki Mitachi, Yoshito Sasaki, Yasuo Ishii, Takayoshi Watanabe

Fukushima Environmental Safety Center, Japan Atomic Energy Agency, Fukushima 963-7700, Japan

ARTICLE INFO

Article history:
Received 30 April 2015
Received in revised form
14 April 2016
Accepted 16 April 2016
Available online 4 May 2016

Keywords:
Radiocesium
Input and output budgets
Mountainous forest
Forest ecosystem
TEPCO's Fukushima Dai-ichi NPP accident

ABSTRACT

Estimations of radiocesium input and output concerning the forest floor within a mountain forest region have been conducted in the north and central part of the Abukuma Mountains of Fukushima, northeast Japan, after a 2–3 year period following the TEPCO Fukushima Dai-ichi nuclear power plant accident. The radiocesium input and output associated with surface washoff, throughfall, stemflow, and litterfall processes at experimental plots installed on the forest floor of evergreen Japanese cedars and deciduous Konara oaks have been monitored. Despite the high output potential in the mountainous forest of Fukushima, the results at both monitoring locations show the radiocesium input to be 4–50 times higher than the output during the summer monsoon in Fukushima. These results indicate that the radiocesium tends to be preserved in the forest ecosystem due to extremely low output ratios (0.05%–0.19%). Thus, the associated fluxes throughout the circulation process are key issues for the projecting the environmental fate of the radiocesium levels, along with the subsequent reconstruction of life emphasized within the setting.

1. Introduction

TEPCO's Fukushima Dai-ichi nuclear power plant (FDNPP) accident is one of the most severe accidents that has ever been experienced in the history of nuclear energy. Most of the contaminated area via the radioactive material released from the FDNPP is a mountainous forest, which covers approximately 70% of the land area of Fukushima Prefecture (MAFF, 2014). Compared with the physical geography among Belarus, Ukraine, and Fukushima, the latter is characterized by a high precipitation and mountainous landform (National Astronomical Observatory of Japan, 2014). This implies a high potential for an outflow of land-forming surface materials such as soil and litter layers. An understanding of the environmental dynamics of radiocesium is, hence, one of the most crucial issues for a recovery of the living environment in and around the subject forested mountain region. ^{137}C is a primary contributor to radiation dose (following the decay of short-lived radionuclides) because of its long half-life of 30 years.

Immediately after the accident, with strong support by local and national governing bodies, an association of universities, and research institutes, a field investigation and monitoring study of the radionuclides released by the accident to characterize their initial distribution and dynamics was launched. Several months after the accident had transpired, investigation results on the contamination levels and environmental dynamics of radiocesium in nearby forested lands had been made open to the public through Internet and scientific publications (e.g., Forestry Agency, 2012). The distribution of radiocesium in the nearby forest ecosystem had evidently changed between 2011 and 2012; concentrations of radiocesium in branches and bark decreased between the two years due to washing-off, with concentrations in leaves notably decreasing from 2011 to 2013. Concentrations in bark, however, remained at the same level between 2012 and 2013. Investigation and monitoring results have altogether shown that the amount of radiocesium in the forest has been essentially constant from 3 years onward subsequent to the accident. This indicates that the radiocesium deposited in the forest has steadily remained within the forest ecosystem (Forestry and Forest Products Research Institute,

* Corresponding author.
E-mail address: niizato.tadafumi@jaea.go.jp (T. Niizato).

http://dx.doi.org/10.1016/j.jenvrad.2016.04.017

2015). Detailed studies have also been performed, which focused on the initial transfer of radiocesium from a canopy to the forest floor via throughfall, stemflow, and litterfall processes (Hisadome et al., 2013; Kato et al., 2012; Teramage et al., 2014; Loffredo et al., 2014) and outflow from a forested mountainous region (Yoshimura et al., 2015; Nishikiori et al., 2015). In addition to the above field-based investigation studies, a modeling assessments of radiocesium fate in a forest ecosystem have been conducted (Hashimoto et al., 2013; Mahara et al., 2014). Hashimoto et al. (2013) simulated the spatiotemporal dynamics of radiocesium deposited in evergreen needle leaf and deciduous broadleaf forests in Japan using of the RIFE model (Shaw and Belli, 1999) developed after the Chernobyl accident in 1986, with its analytical results characterizing radiocesium migrations from trees and surface organic soils to mineral soils over a period of 1–2 years after the accident. Furthermore, Mahara et al. (2014) proposed a numerical model to predict changes in the concentration of ^{137}Cs in tree rings of Konara oak and Sugi (Japanese cedar). Modeling results showed the difference in temporal changes of the concentration profiles between the xylem of Konara and Sugi after the accident. Concentrations were ultimately found unaffected by root uptake if an active root system occurred 10 cm below the soil.

The aforementioned studies treated the migration and transfer processes of radiocesium in a forest ecosystem separately, thus the aggregate behavior of radiocesium in the ecosystem, as a whole, maintains an appreciable degree of ambiguity. As such, an "integrated" understanding of the total behavior of radiocesium (i.e., the input and output budgets of radiocesium and its temporal changes in the ecosystem) can only provide a sound scientific basis for effective remediation of the subject contaminated land area and promotion of an effective intervention strategy to regain the forest ecosystem as a viable setting wherein biota, production, and recreation once again thrive.

The radiocesium initially deposited in a forested area will reach and accumulate on a forest floor via throughfall, litterfall, and stemflow processes. Subsequently, the material will be transported from the forest floor through surface washoff as dissolved and particulate-bond state. Therefore, an assessment is provided herein with regard to input and output budgets of radiocesium within a forested area with the forest floor of particular emphasis to clarify whether the forest floor behaves as a sink (input greater than output) or a source (output greater than input) of the contamination.

2. Materials and methods

2.1. Study area

The subject investigation and monitoring have been conducted at two separate districts (Sakashita and Ogi) of cool-temperate mountainous forests within the Abukuma Mountains, the east of Fukushima Prefecture, Japan. Levels of radioactive contamination in both districts measured 1000–3000 kBq m^{-2} in total radiocesium deposition (^{134}Cs + ^{137}Cs, as of July 2, 2011) via airborne monitoring results (Ministry of Education, Culture, Sports, Science & Technology in Japan, 2015).

The Sakashita district, which is located near the ridge of the Abukuma Mountains, is 34.5 km northwest of the FDNPP (Fig. 1). The mean annual precipitation in this district over the past 30 years (1981–2010) is 1221.7 mm yr^{-1} at the Yamakiya meteorological station, located 2.7 km northwest of the district (Ministry of Land, Infrastructure, Transport and Tourism, 2015). The district is mainly covered by deciduous broad-leaved trees of Konara oak (*Quercus serrata*), Mizunara oak (*Quercus cripspula*), and Japanese chestnut (*Castanea crenata*), except on the southern edge of the forest where Japanese red pine (*Pinus densiflora*) trees are dominant. The average tree height and tree density of canopy layers are 11.2 m and 790 ha^{-1}, respectively. Most of the forest floor is covered with litter composed mainly of fallen branches and leaves of deciduous broad-leaved trees. The thickness of the litter layer is usually 1–3 cm, but is typically over 5 cm around the trunk of a tree. The undergrowth cover, such as mountain azalea (*Rhododendron kaempferi*) and bamboo grass (*Sasa nipponica*), ranged from 35% to 60%. Brown forest soil (andosol and cambisol in IUSS Working Group WRB, 2014) is most common in the Sakashita district with an organic horizon of 3.2 cm (range of 1.0–9.0 cm) and an A horizon of 9.5 cm (range 4.0–12.5 cm) in the average thickness. Andosols with a thick A horizon (range 12.5–40.0 cm thick) were consistently present at the foot of the mountain slope. The soil down to a 5 cm depth is sandy-loam to loam in conventional textural classes.

The Ogi district, which is located on the eastern mountainside slope of the Abukuma Mountains, is 14 km southwest of the FDNPP (Fig. 1). The mean annual precipitation over the past 30 years (1981–2010) is 1465.1 mm yr^{-1} at the Kawauchi meteorological station, 8.7 km west of the Ogi district (JMA, 2015). Evergreen coniferous trees (Japanese cedar; *Cryptomeria japonica*), which prominently exist within an evenly aged mature plantation display a tree density of 740 ha^{-1} and an average 21.3 m tree height for the canopy layer. Almost the entire forest floor is covered with litter such as fallen needle leaves, bark fragments, and cedar tree cones. The thickness of the litter layer is usually 3–4 cm with sparsely development of undergrowth, such as mulberry (*Morus australis*) and lindera (*Lindera praecox*), widely observed throughout the area except on the edge of the forest. The most common soil type in the Ogi district is Brown forest soil (andosol and cambisol in IUSS Working Group WRB, 2014) with an organic horizon of 4.4 cm (range 2–8 cm) and an A horizon of 19.0 cm (range 10–29 cm) in average thickness. The textural class of the soil down to a level of 5 cm is silt-loam to loam.

2.2. Monitoring and sampling

Two experimental plots for monitoring were installed in the mountain forest of the Sakashita district, on a crest slope (KE-plot) and a side slope (KW-plot) of a valley-head area that face west (Fig. 1). Both experimental plots are located on rectilinear and straight slopes, and have common features of a physical geography except for slope angle (Table 1). The 86%–99% of the forest floor in the two plots is covered with litter layer. In the mountain forest of the Ogi district, one plot of KA-plot was installed on a west-facing side slope of a valley-head area (Fig. 1, Table 1). The 91%–97% of the forest floor in the KA-plot surface is covered with a litter layer. The geomorphic feature of the KA-plot is similar to that of the KW-plot, but the forest type is markedly different.

Each experimental plot has a rectangular shape, whose long side orients to the dip direction of the slope, and is surrounded with stainless-steel boards to prevent the transportation of particulate matter and the flow of surface runoff water into the plot from the outside (Fig. 2). The particulate matter, which is composed of soil particles and fine litter fragments, accumulated in an 18 L stainless-steel catchment box installed at the bottom end of the plot. Surface runoff water that drained from the plot likewise flowed into the box with its associated overflow running into a 200 L catchment tank connected to the box via a pipe. After removal of a large litterfall from the catchment box, the relatively coarser particulate matter was collected by a trowel, with finer matter collected as turbid water mixed within the box. The turbid water was filtered through a 0.45 μm pore size Durapore® hydrophilic PVDF membrane filter (HVLP04700, Merck Millipore, Massachusetts, USA) in a laboratory. The particulate matter collected from the catchment box was

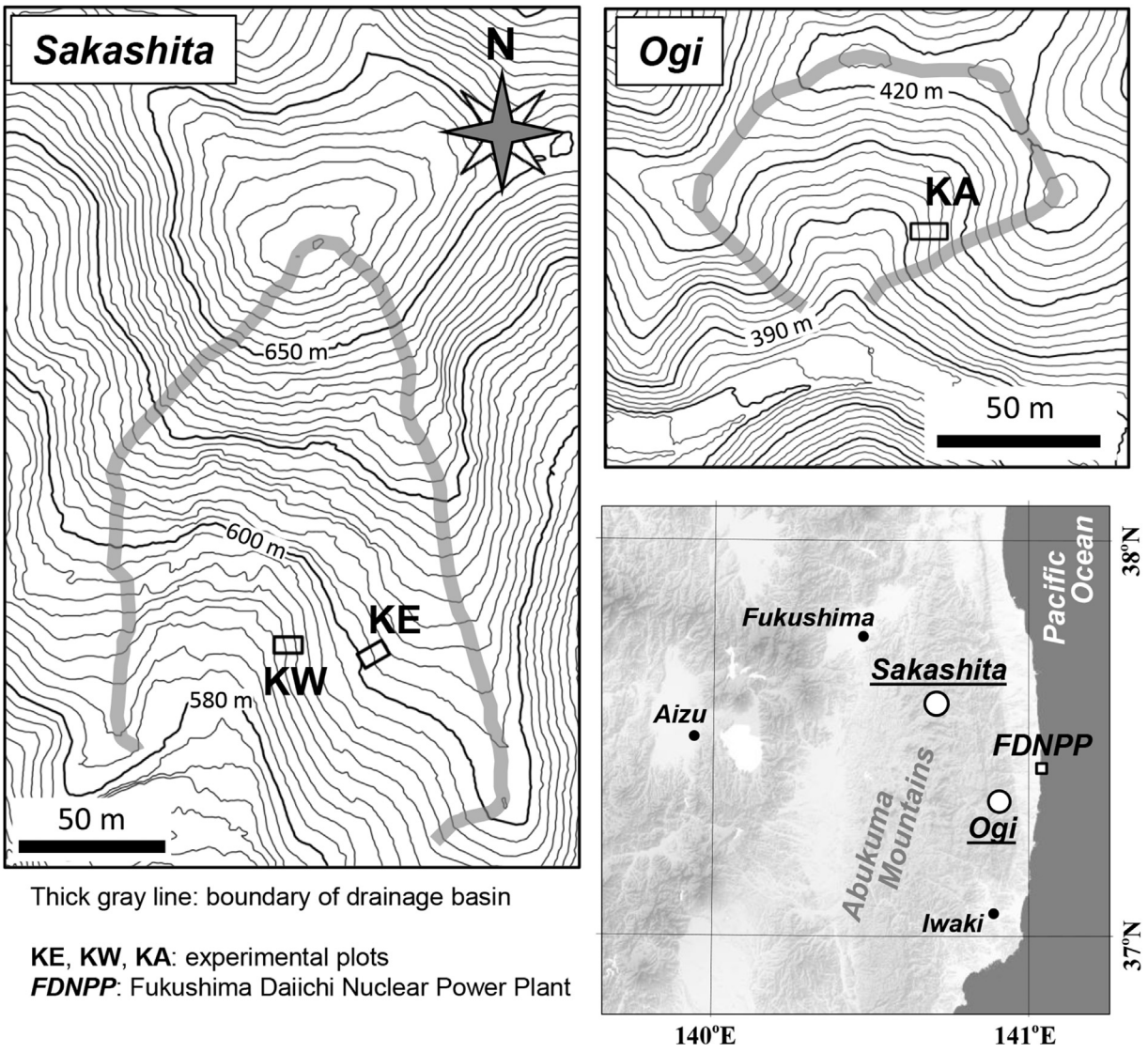

Fig. 1. Location of the study site. The topographic data were created based on the results of an airborne laser survey conducted by the Geospatial Information Authority of Japan.

Table 1
Characteristics of the experimental plot.

District	Sakashita		Ogi
Plot	KE-plot	KW-plot	KA-plot
Elevation (m)	606	590	385
Plot area (m^2)	66 (6.0 m × 11 m)	60 (6.0 m × 10 m)	51 (4.6 m × 11 m)
Slope angle	11–15° W	27–30° WSW	28–31° W
Forest type	Deciduous broad-leaved		Evergreen conifer
Dominant tree species	Konara oak (*Quercus serrata*)		Japanese cedar (*Cryptomeria japonica*)
Tree density[a] (ha^{-1})	920	740	710
Tree height[b] (m)	11.6	10.9	22.7
Forest floor cover (%) by litter layer	91 (early June)	86 (early June)	91 (early June)
	99 (late Nov.)	94 (late Nov.)	97 (late Nov.)
^{137}Cs inventory[c] (kBq m^{-2})	497	497	487

[a] Tree density was the number of trees composed of a canopy layer.
[b] Tree height was on average in the realm of 1440 m^2, 1080 m^2, and 2500 m^2 surrounding the KE-, KW-, and KA-plots, respectively.
[c] The inventory of ^{137}Cs was obtained from the Sixth Airborne Monitoring Survey (as of Dec. 28, 2012) by MEXT (2015) and decay-corrected to April 1, 2013.

weighted after drying under 105 °C during 24 h for the coarse particulate matter and under 90 °C to the constant weight for the filter residues. Those samples were homogenized by hand stirring with a dispensing spoon, and then packed and sealed in a polystyrene container (U-8) for radioassay per sampling date. The sum weight of the residues on the filter and the coarse particulate matter were treated as the gross weight of the particulate matter washed off from the plot.

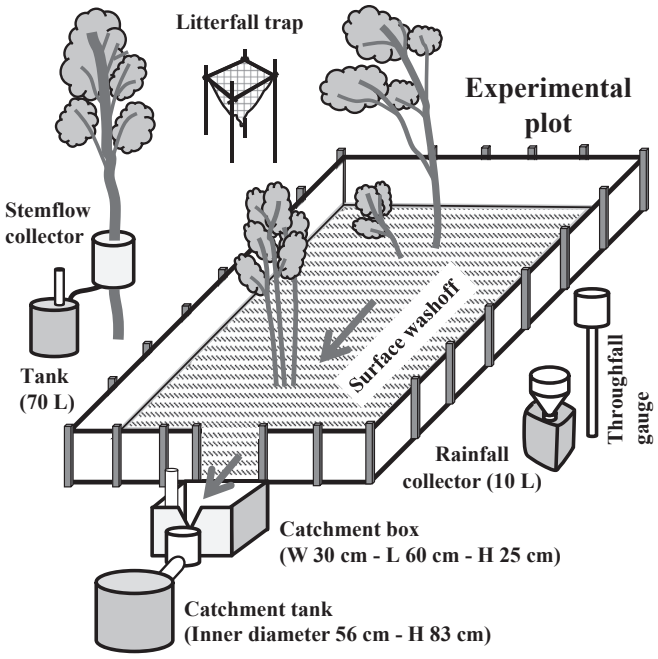

Fig. 2. Overview of the experimental plot.

Water volumes of surface runoff drained from the plots were estimated by subtracting throughfall of each plot from inflow water in the catchment box and the tank because the boxes were uncovered. The inflow water volumes were calculated from the water level in the catchment box and the tank. Water samples for radioassay of the inflow water were collected in a 500 mL polypropylene bottle from the catchment tank after mixing in the tank. The water collected in 2014 was filtered using the 0.45 μm pore size filter as mentioned above but the water collected during 2013 was non-filtered.

To monitor throughfall, a data logging rain gauge was installed beside each of the KE-, KW-, and KA-plots approximately 1.0 m above the forest floor. The funnel of the rain gauge had an area of 0.0214 m^2 and was covered with a metal mesh to prevent contamination by litter material. The throughfall water via the funnel was stored in a polypropylene sampling bottle connected to the rain gauge by tubing. The throughfall water was collected in the 500 mL bottle and filtered using the same method described above except for the samples in the 2013 KA-plot that are non-filtered. For data loss due to a malfunction of the rain gauge, the throughfall of the KA-plot after July 15, 2014 was estimated based on the ratio of the throughfall to gross precipitation in 2013 monitored in the KA-plot.

Rainfall gauges for measuring precipitation outside the forest were installed in the Sakashita and Ogi districts. The specification of the rainfall gauge was the same as that for throughfall, with the distance from the forest edge being approximately 8 m for Sakashita and 5 m for Ogi. A rainfall collector with a funnel was connected directly to a polypropylene 10 L sampling tank and was installed adjacent to the rainfall gauge, with a height of 50 cm above the ground floor. The non-filtered 500 mL rainfall water was separated from the collected water for the measurement of radiocesium after rigorous mixing in the sampling tank.

The experimental plots each included three installed stemflow collectors beside the plots at approximately a 1.5 m height above the forest floor (Table 2). To collect the stemflow water, a rubber or vinyl collar was mounted, wrapping around the stem of the trees. After stripping off an outer bark layer, the collar was fastened with metal staples, attached to a drain tube, and sealed to a trunk with a caulking compound. The stemflow water ran into a 70 L polypropylene tank through the drain tube. The amount of water was estimated by the water level in the tank using a relational curve between the water level and the storage volume that had been determined in a laboratory. Stemflow (L m^{-2}) was calculated by dividing the amount of stemflow water (L) by a crown projection area (m^2). The crown projection area was calculated on an image processing and analysis program (ImageJ; Schneider et al., 2012) after scanning of a crown projection diagram into the ImageJ. The crown projection diagram was drawn from four or more measurements of horizontal distance from a trunk to outer extremities of the tree crown.

After sampling of the stemflow water from the tank, the inner walls were cleaned with a paper towel. The stemflow water was collected in the 500 mL bottle from the collector tank after rigorously stirring the stored water in the tank. Non-filtered water samples were provided for radioassay in the case of the stemflow water collected in 2013. Regarding the stemflow water samples of 2014, the filtered samples were also prepared in the same method as the surface runoff water to remove fine organic fragments from the stemflow water.

Litterfall was collected using rectangular pitfalls dug in the forest floor with 20 cm depth whose bottom areas were 0.12 and 0.16 m^2 in the KE- and KW-plots, respectively. Litterfall in the KA-plot was collected using funnel-shaped litter traps of 1 m^2 steel pipe frame coated with polyethylene at 1 m height. Litterfall samples were weighted after drying under 90 °C for 12 h and crushed into fine fragments using a food processor before packed in U-8 containers for radioassay.

Litterfall collection was performed from middle October to early December in the year 2014. No rainfall was observed during the sampling period of litterfall in the KE- and KW-plots. Associated field surveys and monitoring efforts have been performed mainly during Fukushima's summer monsoon from April to November, in the years 2013–2014 (Fig. 3). This monthly span was chosen as most appropriate for research due to rainfall acting as the principal cause for chemical substance migration within a forested area. Samples of the particulate matter, surface runoff, throughfall, and stemflow waters were collected within 2- to 8-week intervals in correlation to precursory rainfall events.

2.3. Radiocesium measurements

The activity of ^{137}Cs was determined by a Ge-semiconductor detector (GMX40P4-76 germanium detector, Seiko EG&G ORTEC, Tokyo, Japan) coupled with a multichannel analyzer that employed counts at the 662 keV peak. The detection limit of the detector was on the order of 10^2 Bq kg^{-1} for 600 s of particulate matter measurement packed in a U-8 container. In the case of the water sample in the 500 mL bottle, the detection limit of the detector ranged from 1.42 to 3.89 Bq L^{-1} and from 3.29×10^{-1} to 5.06×10^{-1} Bq L^{-1} for 1 h and 15 h measurements, respectively. In addition, the detection limit of the water sample packed and sealed in a 2 L Marinelli bottle ranged from 2.38×10^{-2} to 2.62×10^{-2} Bq L^{-1} for 63 h measurement. The radioactivities reported herein were corrected for radioactive decay with respect to April 1, 2013. The ^{137}Cs activities of the particulate matter and the litterfall are shown in dry weight.

2.4. Calculation of radiocesium input and output

The transportation of the particulate matter from the experimental plot was accompanied by the washoff of particulate-bond ^{137}Cs. The washoff of the particulate-bond ^{137}Cs was calculated by multiplying the weight of the particulate matter by its ^{137}Cs activity

Table 2
Characteristics of trees to which stemflow collectors were mounted.

District	Plot	Stemflow collector	Species	Height[a] (m)	D_{BH}[a] (cm)	Crown projection area[b] (m^2)
Sakashita	KE-plot	KE-1	Aspen	13.9	31.5	19.4 ± 1.2
		KE-2	Japanese chestnut	8.9	17.8	12.9 ± 0.9
		KE-3	Japanese chestnut	10.6	22.0	11.5 ± 0.9
	KW-plot	KW-1	Konara oak	16.1	28.0	24.0 ± 1.3
		KW-2		9.1	11.1	32.5 ± 1.4
		KW-3		9.7	13.1	38.8 ± 1.6
Ogi	KA-plot	KA-1	Japanese cedar	22.2	31.5	8.3 ± 0.8
		KA-2		24.8	42.3	13.0 ± 0.9
		KA-3		23.3	33.1	8.8 ± 0.8

D_{BH}: Tree diameter at a height of 1.3 m calculated from tree girth.
[a] The measurement errors in tree height and D_{BH} are ±0.5 m and ±0.3 cm, respectively.
[b] The errors are derived from the distance measurements on a field investigation.

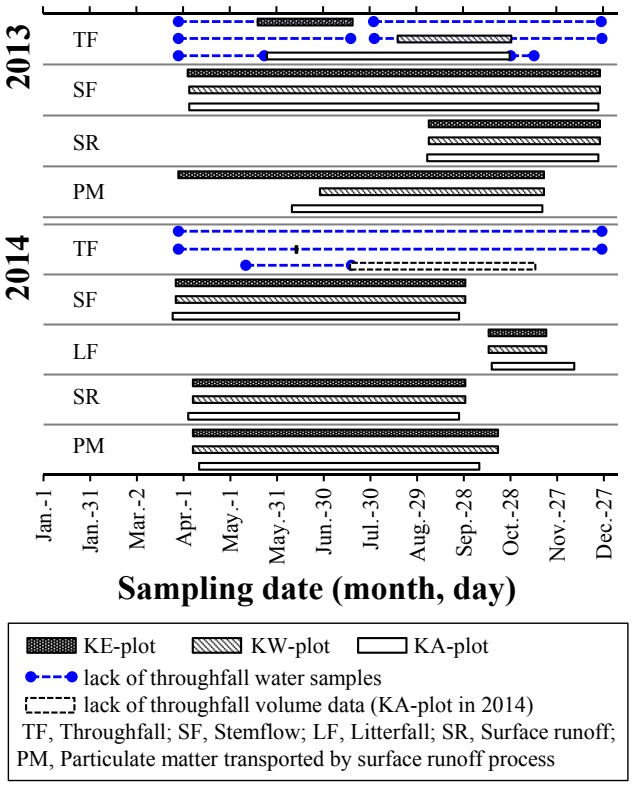

Fig. 3. Monitoring period at each experimental plot.

and then dividing this value by the plot area. The washoff ratio of the particulate-bond ^{137}Cs was calculated using ^{137}Cs inventories obtained from the Sixth Airborne Monitoring Survey (MEXT, 2015, Table 1).

The dissolved ^{137}Cs flowing into the catchment box and the tank was composed of throughfall and surface washoff components because the box had no lid. The surface washoff component was estimated from an end-member mixing analysis equation (Leibundgut et al., 2009). The mass balances of water and dissolved ^{137}Cs flowing into the catchment box and the tank were determined as follows:

$$Q_T = Q_{TF} + Q_{SR} \text{ (mass balance of water) and}$$

$$C_T\, Q_T = C_{TF}\, Q_{TF} + C_{SR}\, Q_{SR} \text{ (mass balance of dissolved } ^{137}\text{Cs)},$$

where Q_T, Q_{TF}, and Q_{SR} indicate the water volume of the catchment box and tank, throughfall, and surface runoff water, respectively. C_T, C_{TF}, and C_{SR} are the ^{137}Cs activities in the catchment box and tank, throughfall, and surface runoff waters, respectively. The output of the dissolved ^{137}Cs via surface washoff was calculated by multiplying the volume of the surface runoff water by its ^{137}Cs activity and then dividing this value by the plot area.

The input of ^{137}Cs via throughfall was calculated by multiplying of the throughfall by its ^{137}Cs activity. The ^{137}Cs activities of stemflow and litterfall were determined for each sample. The volume-weighted mean ^{137}Cs activities of the stemflow water and litterfall were computed by summing the ^{137}Cs amounts of individual stemflow and litterfall samples during the study period and then dividing this value by the total amount of the stemflow water and weight of the litterfall. The input of ^{137}Cs via stemflow was calculated by multiplying the mean activity by the amount of the stemflow water. The deposition of ^{137}Cs through the litterfall process was calculated by multiplying the mean activity by the total weight of litterfall during the study period and then dividing this value by the litterfall trap area.

The ^{137}Cs input and output budges during the summer monsoon season were calculated by summing up daily flux of the different input and output processes for the number of days in the monsoon season (April–November). The daily fluxes were calculated by dividing ^{137}Cs input and output during monitoring period by the number of monitoring days.

3. Results and discussion

3.1. Input via throughfall, stemflow, and litterfall processes

3.1.1. Throughfall

Table 3 shows the gross precipitation, throughfall, and ^{137}Cs activity for the filtered and non-filtered throughfall water samples collected at different experimental plots and periods. The ratios of throughfall to gross precipitation in 2013 were 74% for the KE-plot, 65%–80% for the KW-plot, and 47%–86% for the KA-plot. The activities of the non-filtered and filtered samples were 2.70–7.29 Bq L^{-1} and 0.419–0.957 Bq L^{-1}, respectively. Therefore, most of the activity of the non-filtered water was attributed to fine fragments of litter contained in the water samples, which ultimately filter residues provided through the litterfall process. Thus, the ^{137}Cs inputs via the throughfall process in the KW- and KA-plots were 171 Bq m^{-2} for two and a half months in 2013 and 89 Bq m^{-2} for three months in 2014, respectively. The ^{137}Cs input in the KE-plot was assumed to be similar to that in the KW-plot because the KE-plot was adjacent to the KW-plot. Furthermore, the activities of the rainfall water samples, which were collected during two summer months in 2013, were below the detection limit (<1.82 Bq L^{-1}) in the Sakashita (KE- and KW-plots) and Ogi (KA-plot) districts.

Table 3
^{137}Cs activity of the throughfall water and ^{137}Cs input via throughfall during different sampling periods.

Plot	Sampling period[a]	Gross precipitation (mm)	Throughfall			
			Throughfall (mm)[b]	^{137}Cs activity (Bq L^{-1})		^{137}Cs input[c] (Bq m^{-2})
				Non-filtered	Filtered	Filtered
KE-plot	May 19–July 19, 2013	106.4	79.2	*nd* (*<2.22*)	–	–
KW-plot	Aug. 17–Oct. 17, 2013	170.1	136.8	6.80 ± 0.90	0.957 ± 0.129	131 ± 18
	Oct. 17–Oct. 29, 2013	95.8	62.6	4.86 ± 0.85	0.642 ± 0.123	40 ± 8
	10:40–14:30 June 12, 2014	13.3	5.4	4.63 ± 0.53	*nd* (*<0.338*)	–
KA-plot	May 25–July 25, 2013	92.7	79.6[d]	2.70 ± 0.73	–	–
	July 25–Oct. 16, 2013	387.5	182.0[e]	7.29 ± 0.89	–	–
	Oct. 16–Oct. 28, 2013	164.6	84.8	*nd* (*<2.02*)	–	–
	July 17–Aug. 18, 2014	190.1	(*102.7*)	*nd* (*<1.80*)	–	–
	Aug. 18–Nov. 13, 2014	394.4	(*213.0*)	–	0.419 ± 0.124	(*89 ± 26*)

nd = not detected. Figures in parentheses are detection limits (Bq L^{-1}).
[a] The number of samples in each sampling period is one.
[b] Figures in parentheses are estimated throughfall based on the ratio of the throughfall to gross precipitation in 2013 because data were lost due to a malfunction of the rain gauge.
[c] Figures in parentheses are estimated ^{137}Cs inputs based on the ratio of throughfall to gross precipitation in 2013.
[d] Data loss for nine days. Gross precipitation was 11.6 mm during the data-loss period.
[e] Data loss for eight days. Gross precipitation was 41.6 mm during the data-loss period.

3.1.2. Stemflow

The ratios of stemflow to gross precipitation in 2013 and 2014 were 8.6% for the KE-plot, 2.0%–3.7% for the KW-plot, and 4.5%–5.0% for the KA-plot. Before estimating the ^{137}Cs input on the forest floor due to stemflow, the temporal change in the amount of stemflow and its associated ^{137}Cs activity in the experimental plot was assessed. The activity tended to decrease with a wide range of variation during the monitoring period from 2013 to 2014, and higher activity levels were observed when the stemflow amounts were noticeably low (Fig. 4). The mean ^{137}Cs activity of non-filtered stemflow water collected in 2013 was two-times higher than that in 2014 (Table 4), and the range of in the 2014 activity was narrower than in 2013, although the seasonal variation was not clear. The differences in the ^{137}Cs activities of non-filtered and filtered stemflow water samples were within the statistically expected error range in 2014, with the exceptions of four samples collected on July 28 in the KW-plot, and on July 17, July 29, and Sep. 25 in the KA-plot (Fig. 4). Based on these results, the litterfall contamination of the stemflow water had a negligible effect for the water samples collected in 2014. Assuming a similar scenario for the stemflow water samples collected in 2013, the ^{137}Cs input to the forest floor through the stemflow process in 2013 was calculated using the mean ^{137}Cs activity for the non-filtered samples of stemflow water. Thus, the ^{137}Cs inputs via the stemflow process for nine months in 2013 were 981, 182, and 687 Bq m^{-2} for the KE-, KW-, and KA-plots, respectively (Table 4). The ^{137}Cs inputs for six months in 2014 were determined based on the mean activities of the filtered samples; the resulting inputs of ^{137}Cs were 474, 82, and 237 Bq m^{-2} for the KE-, KW-, and KA-plots, respectively (Table 4).

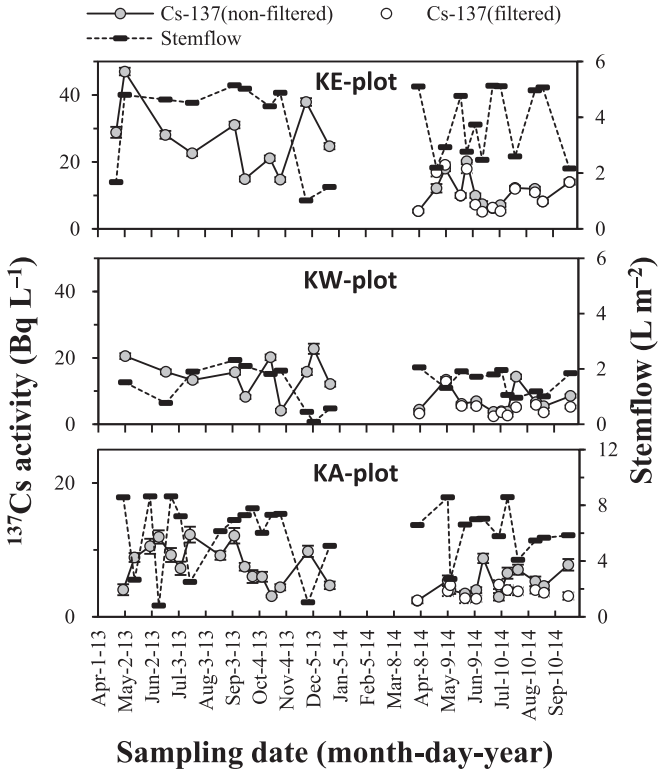

Fig. 4. Stemflow and its ^{137}Cs activity. The ^{137}Cs activity is a volume-weighted mean at each experimental plot (N = 3 for each plot).

3.1.3. Litterfall

The volume-weighted means of the litterfall ^{137}Cs activities and the ^{137}Cs depositions through the litterfall process in the each plot during the sampling period are shown in Table 5. The period of study was approximately equivalent to a major leaf-fall period (October–November) in the deciduous broad-leaved forests of the KE- and KW-plots.

The amount of litterfall has significant seasonal variation in broad-leaved and cedar forests (Hisadome et al., 2013; Okada et al., 2015; Endo et al., 2015; Kato et al., 2015). Hisadome et al. (2013) reported seasonal variation in litterfall and resultant radiocesium deposition through the litterfall process by sampling at intervals of 1–2 weeks from August 2011 to May 2012 in the mixed broad-leaved and mature cedar forests of the Yamakiya district, within 3 km of the Sakashita district. Kato et al. (2015) investigated the canopy interception of radiocesium and its subsequent transfer to the forest floor via the litterfall process using the same experimental plots as Hisadome et al. (2013). The tree density of the cedar forest was 1250 ha^{-1}, and that of the mixed broad-leaved forest was 2500 ha^{-1}; Japanese oak (*Quercus* spp.) and Japanese red pine (*Pinus densiflora*) were the dominant species (Kato et al., 2015). These results indicated that the litterfall mass in the leaf-fall period (October–November 2011) accounted for approximately 60% and 40% of all litterfall from August–December of 2011 in the mixed

Table 4
Mean ^{137}Cs activity of the stemflow water and ^{137}Cs input via stemflow at each experimental plot.

Plot	Period	^{137}Cs activity (Bq L^{-1})		^{137}Cs input (Bq m^{-2})	
		Non-filtered	Filtered	Non-filtered	Filtered
KE-plot	Apr. 4–Dec. 25, 2013	26.1 ± 0.3 (N = 10)	–	981 ± 12	–
	Mar. 27–Sept. 29, 2014	10.1 ± 0.2 (N = 13)	9.68 ± 0.20 (N = 13)	496 ± 9	474 ± 10
KW-plot	Apr. 5–Dec. 25, 2013	13.6 ± 0.3 (N = 10)	–	182 ± 3	–
	Mar. 27–Sept. 29, 2014	6.62 ± 0.15 (N = 11)	4.93 ± 0.15 (N = 11)	111 ± 3	82 ± 3
KA-plot	Apr. 5–Dec. 24, 2013	7.32 ± 0.23 (N = 16)	–	687 ± 22	–
	Mar. 25–Sept. 25, 2014	5.24 ± 0.20 (N = 12)	3.21 ± 0.18 (N = 12)	387 ± 14	237 ± 13

N = number of samples.

Table 5
Mean ^{137}Cs activity of litterfall and ^{137}Cs deposition via litterfall at each experimental plot.

Plot	Litterfall trap area (m^2)	Sampling period	Litterfall		
			Weight (g)	^{137}Cs activity (kBq kg^{-1})	^{137}Cs deposition (kBq m^{-2})
KE-plot	0.12	Oct. 14–Nov. 20, 2014	146	6.88 ± 0.04 (N = 2)	8.36 ± 0.05
KW-plot	0.16	Oct. 14–Nov. 20, 2014	112	2.43 ± 0.02 (N = 3)	1.69 ± 0.01
KA-plot	1.00	Oct. 16–Dec. 8, 2014	145	15.3 ± 0.1 (N = 3)	2.22 ± 0.01

N = number of samples.

broad-leaved and cedar forests, respectively (Hisadome et al., 2013).

Okada et al. (2015) monitored litterfall ^{137}Cs in red pine (36- to 54-year-old) and deciduous broad-leaved (43-year-old) forests after the FDNPP accident from October 2012 to December 2013 in Kawauchi Village, 2 km west of the Ogi district. Japanese oak was the dominant species in this forest. The tree density of the deciduous broad-leaved forest was 1413 ha^{-1}, and the average trunk diameter was 14.2 cm. The results revealed the seasonality of litterfall ^{137}Cs deposition related to the leaf fall of the dominant tree species. The litterfall in the leaf-fall period (November 2013) accounted for approximately 59% of the litterfall mass from April–December in 2013.

Endo et al. (2015) estimated the annual transportation of ^{137}Cs from the forest canopy to the floor via litterfall, throughfall, and stemflow in two deciduous and cedar plantation forests of the Ryozen district, which is 20 km north of the Sakashita district, from October 2012 to September 2013. The deciduous forest consisted of a mixture of broad-leaf species, including oak (*Quercus* spp.) and maple (*Acer* spp.) with a tree density of 800–1300 ha^{-1}. The cedar plantation was approximately 50 years old with a tree density of 2100 ha^{-1}. The authors observed that ^{137}Cs transportation via litterfall increased in the leaf-fall period simply due to the increased amount of litterfall; the litterfall mass in the leaf-fall period (October–November) accounted for approximately 55% and 60% of the litterfall from April–December in the deciduous broad-leaved and cedar forests, respectively. By monitoring monthly litterfall biomass and its ^{137}Cs activity, Endo et al. (2015) showed that the seasonal variation in ^{137}Cs fluxes from the canopy to the forest floor mainly originated from changes in litterfall biomass, not from differences in the ^{137}Cs activity of the litterfall.

Based on the abovementioned studies, the amount of litterfall during the leaf-fall period (October–November) in the deciduous broad-leaved forests of the KE- and KW-plots and the cedar forest of the KA-plots were inferred to be 50%–60% and 40%–60% of the litterfall in April–December of 2014, respectively. Based on the results of monitoring in the Yamakiya district and Tochigi Prefecture of central Japan (180 km southwest of the FDNPP), the litterfall ^{137}Cs activities remained at the same level after October 2011 in deciduous broad-leaved and cedar forests (Hisadome et al., 2013) and generally decreased after July 2011 for Japanese cypress (*Chamaecyparis obtusa*) plantation forest (Teramage et al., 2014). Thus, assuming that the amounts of litterfall in the KE-, KW-, and KA-plots in 2013 were the same as in 2014, the 2013 ^{137}Cs depositions via the litterfall process in these plots were equal to or larger than those in 2014. From the discussion above, the respective amounts of litterfall and resultant ^{137}Cs deposition from April–December 2014 were estimated to be 243–292 g and 13.9–16.7 kBq m^{-2} for the KE-plot, 187–224 g and 2.84–3.40 kBq m^{-2} for the KW-plot, and 242–363 g and 3.70–5.55 kBq m^{-2} for the KA-plots.

3.2. Output via the surface runoff process

The transporting agents of ^{137}Cs in the surface runoff process on the forest floor were surface runoff water and fine-grained particulate matter, which was mainly composed of fine litter fragments and soil particles derived from forest floor erosion. It is reasonable to assume that ^{137}Cs in the surface runoff water exists as a dissolved chemical substance, whereas in particulate matter, ^{137}Cs is strongly sorbed and fixed on mica-like minerals and other soil components (Tamura and Jacobs, 1960; Sawhney, 1970; Comans et al., 1991; Ohnuki and Kozai, 2013; Evrard et al., 2015). For these reasons, the ^{137}Cs outputs from the experimental plot via the different transporting agents (surface runoff water and particulate matter) were estimated separately. In the following discussion, the washoff is the ^{137}Cs outputs through the surface runoff process.

Table 6 shows the calculated results of the water inflow and ^{137}Cs input to the catchment box and tank from an end-member mixing analysis (Leibundgut et al., 2009). The amount of water and ^{137}Cs activities for the catchment box and tank, along with the throughfall were measured in the KE-, KW-, and KA-plots. Water inflow and ^{137}Cs input to the catchment box and tank via surface runoff accounted for 65%–69% of the stored water and 94%–98% of the ^{137}Cs input to the box and tank, respectively. The calculated ^{137}Cs washoff as dissolved state from the experimental plots during the different sampling period are shown in Table 7. There was no clear relationship between the activity and amount of surface runoff water during the entire monitoring period. However, for non-filtered water samples, the ^{137}Cs activity of the surface runoff water collected in 2014 tended to be lower than that of runoff water collected in 2013 for each experimental plot (except for the water sample corresponding to October 17–29, 2013 in the KE-plot). This tendency was the same as that observed for the ^{137}Cs activity of

Table 6
Separation of ^{137}Cs inputs to the catchment box and tank.

Plot	Measured						Calculated		
	Catchment box and tank			Throughfall[a]			Surface runoff[a,b]		
	Water volume (L)	^{137}Cs activity (Bq L^{-1})	^{137}Cs inventory (Bq)	Water inflow (L)	^{137}Cs activity (Bq L^{-1})	^{137}Cs input (Bq)	Water inflow (L)	^{137}Cs activity (Bq L^{-1})	^{137}Cs input (Bq)
KE-plot	94.6	14.5 ± 0.8	1370 ± 73	30.8	0.963 ± 0.108	29.6 ± 3.3	63.8	21.0 ± 1.1	1340 ± 73
KW-plot	98.3	18.6 ± 0.7	1820 ± 71	30.8	0.963 ± 0.108	29.6 ± 3.3	67.5	26.6 ± 1.0	1790 ± 71
KA-plot	93.0	2.53 ± 0.37	235 ± 35	32.6	0.419 ± 0.124	13.7 ± 4.0	60.4	3.66 ± 0.58	221 ± 35

[a] Water inflow and ^{137}Cs input to the catchment box and tank.
[b] Period for estimation is Sept. 6–Oct. 29, 2013 at the KE- and KW-plots and Aug. 18–Oct. 22, 2014 at the KA-plot.

Table 7
Measured ^{137}Cs activities of the catchment tank water and calculated ^{137}Cs washoff as dissolved state during different sampling periods.

Plot	Sampling period	Catchment box and tank (measured)			Surface washoff (calculated)	
		Volume (L)	^{137}Cs activity (Bq L^{-1})		^{137}Cs output (Bq m^{-2})	
			Non-filtered	Filtered	Non-filtered	Filtered
KE-plot	Sept. 6–Sept. 27, 2013	38.0	16.6 ± 1.3	–	9.34 ± 0.74	–
	Sept. 27–Oct. 17, 2013	37.6	14.9 ± 1.3	–	8.30 ± 0.73	–
	Oct. 17–Oct. 29, 2013	19.0	9.55 ± 1.06	–	2.69 ± 0.30	–
	Apr. 7–July 2, 2014	39.5	4.93 ± 0.76	5.46 ± 0.83	2.89 ± 0.45	3.20 ± 0.49
	July 2–July 11, 2014	17.1	4.21 ± 0.71	4.28 ± 0.71	1.07 ± 0.18	1.09 ± 0.18
	July 11–July 28, 2014	11.2	7.54 ± 0.90	7.69 ± 0.97	1.25 ± 0.15	1.28 ± 0.16
	July 28–Aug. 20, 2014	33.4	6.90 ± 0.90	5.41 ± 0.82	3.41 ± 0.44	2.68 ± 0.40
	Aug. 20–Aug. 29, 2014	28.0	8.48 ± 0.96	5.87 ± 0.88	3.52 ± 0.40	2.44 ± 0.36
	Aug. 29–Sept. 29, 2014	10.5	14.0 ± 1.1	13.7 ± 1.2	2.17 ± 0.18	2.13 ± 0.19
KW-plot	Sept. 6–Sept. 18, 2013	24.4	28.3 ± 1.6	–	11.3 ± 0.6	–
	Sept. 18–Oct. 17, 2013	42.0	22.6 ± 1.5	–	15.5 ± 1.0	–
	Oct. 17–Oct. 29, 2013	31.9	9.95 ± 1.10	–	5.20 ± 0.58	–
	Oct. 29–Dec. 25, 2013	23.9	13.0 ± 1.2	–	5.10 ± 0.48	–
	Apr. 7–July 2, 2014	41.8	6.42 ± 0.85	6.60 ± 0.89	4.40 ± 0.59	4.52 ± 0.61
	July 11–July 28, 2014	10.0	12.3 ± 1.1	8.46 ± 1.03	2.01 ± 0.19	1.39 ± 0.17
	July 28–Aug. 20, 2014	27.6	9.88 ± 0.99	6.71 ± 0.91	4.47 ± 0.45	3.04 ± 0.41
	Aug. 20–Aug. 29, 2014	23.0	9.31 ± 1.01	7.62 ± 0.93	3.51 ± 0.38	2.87 ± 0.35
	Aug. 29–Sept. 29, 2014	7.5	13.7 ± 1.2	–	1.67 ± 0.15	–
KA-plot	Sept. 5–Sept. 17, 2013	28.3	11.7 ± 1.3	–	6.13 ± 0.69	–
	Sept. 17–Oct. 18, 2013	57.2	15.5 ± 1.3	–	16.4 ± 1.4	–
	Oct. 18–Oct. 28, 2013	49.3	6.44 ± 0.93	–	5.87 ± 0.85	–
	Apr. 4–June 19, 2014	41.6	*nd* (*<1.87*)	*nd* (*<1.86*)	–	–
	June 19–July 17, 2014	17.1	2.73 ± 0.68	2.75 ± 0.67	0.86 ± 0.21	0.87 ± 0.21
	July 17–July 29, 2014	14.4	4.69 ± 0.84	2.27 ± 0.70	1.25 ± 0.22	0.60 ± 0.19
	July 29–Aug. 28, 2014	28.2	3.56 ± 0.73	2.39 ± 0.74	1.86 ± 0.38	1.24 ± 0.39
	Aug. 28–Sept. 25, 2014	15.9	4.86 ± 0.74	2.76 ± 0.69	1.43 ± 0.22	0.81 ± 0.20

nd = not detected. Figures in parentheses are detection limits (Bq L^{-1}).

stemflow water (Table 4). This implies that the contributions of hydrological pathways became less important as time passed (Teramage et al., 2014). The ^{137}Cs activities of the non-filtered and filtered water samples in 2014 were on the same order of magnitude except for the water sample covering July 11–28, 2014 for the KW-plot. To be precise, the differences in the ^{137}Cs activities of the non-filtered and filtered samples were within a statistically expected error range except for the sample mentioned above. Assuming that the situation was similar in 2013, the 2013 ^{137}Cs washoff from the forest floor was calculated using the ^{137}Cs activities of the non-filtered samples of surface runoff water. The ^{137}Cs washoff of each sampling period were summed to provide the total ^{137}Cs washoff during the monitoring periods in 2013 and 2014. The ^{137}Cs washoff from the forest floor (via surface runoff water) were estimated to be 20.3 Bq m^{-2} (September–October 2013) and 14.3 Bq m^{-2} (April–September 2014) for the KE-plot, 32.1 Bq m^{-2} (September–October 2013) and 16.1 Bq m^{-2} (April–September 2014) for the KW-plot, and 28.4 Bq m^{-2} (September–October 2013) and 5.39 Bq m^{-2} (April–September 2014) for the KA-plot (Table 7).

The weight of the particulate matter transported from the experimental plot during the monitoring period is shown in Table 8. Compared with other input and output processes, the particulate matter transported via surface runoff was characterized by a high ^{137}Cs activity and a relatively lower weight. Therefore, the ^{137}Cs washoff associated with the outflow of particulate matter was extremely low compared to the ^{137}Cs inventory around the experimental plot (Table 8). The sum of the particulate matter weights from 2013 to 2014 in the KW-plot was larger than that of the KE-plot but equal to that of the KA-plot. The forest type, forest floor cover percentage by litter layer as well as the rainfall condition of the KE-plot were similar to those of the KW-plot, except for the slope angle (Tables 1 and 8). The features described above suggest that the slope angle is responsible for the difference in the particulate matter weight between the KE- and KW-plots (Table 1). Rainfall intensity is positively correlated with the amount of soil erosion on a forest floor (Higashi, 1989). In contrast, forest floor cover, such as litter layer and understory less than 50 cm tall,

Table 8
^{137}Cs washoff accompanied by the transportation of particulate matter.

Plot	Period	Gross precipitation (mm)	Particulate matter (g)	^{137}Cs activity[a] (kBq kg^{-1})	^{137}Cs washoff	
					(Bq m^{-2})	(%)[b]
KE-plot	Mar. 29–Nov. 19, 2013	1101[c]	617	26	245	0.05
	Apr. 7–Oct. 20, 2014	1251	259	77	304	0.06
KW-plot	June 28–Nov. 19, 2013	920[c]	617	47	480	0.10
	Apr. 7–Oct. 20, 2014	1251	1112	32	600	0.12
KA-plot	June 10–Nov. 18, 2013	518	1225	21	514	0.11
	Apr. 11–Oct. 8, 2014	914	382	24	176	0.04

[a] Data in 2013 are adopted from Ishii et al. (2015).
[b] The percentage of ^{137}Cs washoff was calculated using the inventory shown in Table 1.
[c] Data from Ministry of Land, Infrastructure, Transport and Tourism (2015).

suppress soil erosion regardless of the rainfall intensity and landform (Tsukamoto, 1989; Hattori et al., 1992; Miura et al., 2003). The forest type and rainfall condition of the KW-plot were different from those of the KA-plot, although their percentages of forest floor cover were similar (Tables 1 and 8). This similarity may account for the same particulate matter weights of the KW- and KA-plots.

A smaller amount of particulate matter transported from the experimental plot indicates a shallower erosion depth in the plot. Base on the ^{137}Cs depth distribution and its temporal changes in the forest soil after the FDNPP accident (Fujii et al., 2014; Takahashi et al., 2015), the shallower erosion depth increased the ^{137}Cs activity of eroded soil particles, even two to three years after the accident. However, it is extremely difficult to explain the differences in the ^{137}Cs activities of the particulate matter based on the differences in particulate matter weight (Table 8), which were less than 1 mm when the weight was converted into the erosion depth, assuming a dry soil density of 1.0 g cm^{-3}.

Using an experimental plot 3 km northwest of the KE- and KW-plots of this study with an area of 110.5 m^2 and a slope of 27.5°, Yoshimura et al. (2015) reported that in a Japanese cedar forest with a mean vegetation cover of 95%, the percentage of the annual rate of ^{137}Cs washoff associated with soil erosion compared to the inventory was 0.07% from July 2011 to November 2012. Using a 3-m^2 plot with a slope of 37–39° in the mountainous forests of the Abukuma Mountains, 47 km north-northwest from FDNPP, Nishikiori et al. (2015) reported that 0.086%–1.1% of the ^{137}Cs inventory in the soil was washed off from May to October 2013. The largest amounts of ^{137}Cs washoff were observed in Japanese cypress forests, followed by deciduous broadleaf, Japanese red pine, and Japanese cedar. The amount of soil loss was relatively larger in the Japanese cypress and deciduous broadleaf forests with little understory and/or organic horizon (forest floor cover; 5%–15%), suggesting that the forest floor covering strongly affects ^{137}Cs washoff (Nishikiori et al., 2015). Compared with the same forest floor cover percentage, this study's estimation was in the range of the pre-existing investigation results despite the differences in forest type and topography. This implies that the protective effect of forest floor cover is an important factor for soil erosion.

3.3. Input and output budgets of ^{137}Cs

The monitoring of the throughfall, stemflow, litterfall, surface runoff water, and particulate matter at the experimental plots was performed mainly during the summer monsoon season in Fukushima Prefecture. However, the monitoring periods varied according to the monitoring item and experimental plots for malfunctions of the monitoring instrumentations (Fig. 3). When comparing the same unit interval, the ^{137}Cs inputs (via throughfall, stemflow, and litterfall) and outputs (via surface washoff) on the forest floor described above were converted to values per 243 days of the monitoring period from April–November (Fig. 5, Table 9).

To summarize the above results, the ^{137}Cs inputs on the forest floors of the experimental plots were 4–50 times higher than the ^{137}Cs outputs from the forest floors (Fig. 5, Table 9). Except for the KW-plot, the sum of the inputs via stemflow and throughfall processes was nearly equal to or higher than the sum of the outputs via the surface washoff in the experimental plots in 2013 and 2014. The most significant contributor to ^{137}Cs input to the forest floor was litterfall, specifically in the KE-plot. The input of ^{137}Cs via litterfall of in the KE-plot was an order of magnitude greater than that in the KW-plot. The ^{137}Cs input from the stemflow in the KE-plot was also higher than that in the KW-plot. Based on air dose rate measurements and geostatistical analysis of the air dose rate distribution in mountainous forested area, Andoh et al. (2015) reported that air dose rates were highly spatially variable and topographically anisotropic, and increased with elevation. These results indicated that more radiocesium was deposited on ridges. This spatial variation may account for the differences in ^{137}Cs input in the KE- and KW-plots.

The rectangular shape of the experimental plot and the smaller width of the catchment box (0.30 m) compared to the width of the lower boundary of the experimental plot (4.6 and 6.0 m; Fig. 2 and Table 1) affect the transport of particulate matter and surface runoff water from the plot to some extent, although the degree of this influence is difficult to estimate. A sheet-like runoff (overland flow) and sheet erosion are idealized concepts that rarely occur (Hillel, 1998). In reality, overland flow on forested hillslopes is discontinuous on patches of hillslope because the root networks of trees and understory vegetation facilitate infiltration (Gomi et al., 2008), and very soon after surface runoff begins to concentrate in small rills with discontinuity in parallel to the contour line and in the downslope direction (Hillel, 1998; Gomi et al., 2008). Thus, the weight of particulate matter and volume of surface runoff water transported from the experimental plot were likely underestimated, although the difference in may be less than one order of magnitude.

4. Conclusion

The input and output budgets of radiocesium in mountainous forests were estimated based on field surveys via the use of experimental plots installed in two different districts of the Abukuma Mountains of Fukushima, Japan. The results show that the inputs of ^{137}Cs on the forest floor were 4–50 times higher than the ^{137}Cs outputs from the forest floor, and that litterfall is the most significant contributor to radiocesium input on the forest floor. ^{137}Cs output was estimated to be 0.05%–0.19% of the ^{137}Cs inventory during Fukushima's monsoon season (April–November). These values primarily fall within the realm of a first-order quantification, however, we could definitively conclude that the output

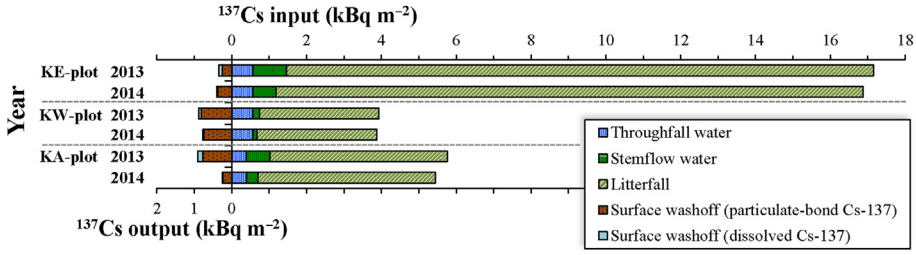

Fig. 5. Input and output budgets for ^{137}Cs at the experimental plots during a summer monsoon season (April–November).

Table 9
Input and output budgets for ^{137}Cs in each experimental plot during summer monsoon from April to November.

Plot	Year	^{137}Cs inventory[a] (kBq m^{-2})	^{137}Cs input		^{137}Cs output		^{137}Cs input/output
			(kBq m^{-2})	(%)[b]	(kBq m^{-2})	(%)[b]	
KE-plot	2013	497.0	17.2	3.45	0.3	0.07	50
	2014		16.9	3.40	0.4	0.08	43
KW-plot	2013	497.0	3.9	0.79	0.9	0.18	4
	2014		3.9	0.78	0.8	0.15	5
KA-plot	2013	487.0	5.8	1.18	0.9	0.19	6
	2014		5.4	1.12	0.2	0.05	22

[a] The inventory of 137Cs was obtained from the Sixth Airborne Monitoring Survey (as of Dec. 28, 2012) by MEXT (2015) and decay-corrected to April 1, 2013.
[b] The percentages compared to the ^{137}Cs inventory of each experimental plot.

of radiocesium from the forest floor is extremely low, with such radiocesium levels tending to be preserved in the forest ecosystem through the present juncture. Thus, the forest floor in the mountainous forest seems to be a sink of radiocesium contamination rather than a source for the contamination of other ecosystems. Hence, the associated fluxes throughout the circulation process in the forest ecosystem are key issues for the projecting the environmental fate of the radiocesium levels, along with the subsequent reconstruction of life emphasized within the setting.

Acknowledgments

The authors thank a local landowner who provides us his hill as our monitoring site in the Sakashita district. We thank Dr. Hiromitsu Saegusa and Mr. Ryuji Takeuchi of the Japan Atomic Energy Agency for their helpful suggestions and technical support during the course of this work. We also thank two anonymous reviewers for many helpful criticism of the manuscript. The gamma-ray measurement was performed at the Sasakino Analytical laboratory, Fukushima Radiation Measurement Group with helpful advice.

References

Andoh, M.A., Koarashi, J., Takeuchi, E., Tsuduki, K., Nishimura, S., Matsunaga, T., 2015. Catchment-scale distribution of radiocesium air dose rate in a mountainous deciduous forest and its relation to topography. J. Environ. Radiact. 147, 1–7.

Comans, R.N., Haller, M., De Preter, P., 1991. Sorption of cesium on illite: non-equilibrium behavior and reversibility. Geochim. Cosmochim. Acta 55, 433–440.

Endo, I., Ohte, N., Iseda, K., Tanoi, K., Hirose, A., Kobayashi, N.I., Murakami, M., Tokuchi, N., Ohashi, M., 2015. Estimation of radioactive 137-cesium transportation by litterfall, stemflow and throughfall in the forests of Fukushima. J. Environ. Radiact. 149, 176–185.

Evrard, O., Laceby, J.P., Lepage, H., Onda, Y., Cerdan, O., Ayrault, S., 2015. Radiocesium transfer from hillslopes to the Pacific Ocean after the Fukushima nuclear power plant accident: a review. J. Environ. Radiact. 148, 92–110.

Forestry Agency, 2012. The Results of Distributional Situation and Analytical Result for the Radionuclide in a Forest (Interim Report). Forestry Agency (in Japanese). http://www.rinya.maff.go.jp/j/press/hozen/110930.html (accessed 17.03.15.).

Forestry and Forest Products Research Institute, 2015. The Results of Distributional Situation and Analytical Result for the Radionuclide in a Forest (Temporal Change until Three and a Half Years after the FDNPP Accident). Forestry and Forest Products Research Institute (in Japanese). https://www.ffpri.affrc.go.jp/press/2015/20150327/index.html (accessed 17.04.15.).

Fujii, K., Ikeda, S., Akama, A., Komatsu, M., Takahashi, M., Kaneko, S., 2014. Vertical migration of radiocesium and clay mineral composition in five forest soils contaminated by the Fukushima nuclear accident. Soil Sci. Plant Nutr. 60, 751–764.

Gomi, T., Sidle, C.R., Miyata, S., Kosugi, K., Onda, Y., 2008. Dynamic runoff connectivity of overland flow on steep forested hillslopes: scale effects and runoff transfer. Water Resour. Res. 44, W08411. http://dx.doi.org/10.1029/2007WR005894.

Hashimoto, S., Matsuura, T., Nanko, K., Linkov, I., Shaw, G., Kaneko, S., 2013. Predicted spatio-temporal dynamics of radiocesium deposited onto forests following the Fukushima nuclear accident. Sci. Rep. 3, 2564. http://dx.doi.org/10.1038/srep02564.

Hattori, S., Abe, T., Kobayashi, C., Tamai, K., 1992. Effect of forest floor coverage on reduction of soil erosion in Hinoki plantations. Bull. For. Prod. Res. Inst. No. 362 1–34 (in Japanese with English abstract).

Higashi, H., 1989. Measurement and analysis of factors for quantification of water-storage capacity of forest land. Bull. Hiroshima Prefect. For. Exp. Stn. No. 23 45–91 (in Japanese with English abstract).

Hisadome, K., Onda, Y., Kawamori, A., Kato, H., 2013. Migration of radiocaesium with litterfall in hardwood-Japanese red pine mixed forest and sugi plantation. J. Jpn. For. Soc. 95, 267–274 (in Japanese with English abstract).

Hillel, D., 1998. Environmental Soil Physics. Academic Press, New York.

Ishii, Y., Abe, H., Niizato, T., 2015. Deposition of radioactive caesium in the Fukushima mountain forests by the Fukushima nuclear power plant accident. In: Proceedings of ICONE-23, 23th International Conference on Nuclear Engineering, May 17-21, 2015, Chiba, Japan. ICONE23-1595.

IUSS Working Group WRB, 2014. World Reference Base for Soil Resources 2014, International Soil Classification System for Naming Soils and Creating Legends for Soil Maps. World Soil Resources Reports, No.106. FAO, Rome.

Japan Meteorological Agency (JMA), 2015. Climate statistics (in Japanese). http://www.data.jma.go.jp/obd/stats/etrn/index.php (accessed 17.03.15.).

Kato, H., Onda, Y., Gomi, T., 2012. Interception of the Fukushima reactor accident-derived ^{137}Cs, ^{134}Cs and ^{131}I by coniferous forest canopies. Geophys. Res. Lett. 39, L20403. http://dx.doi.org/10.1029/2012GL052928.

Kato, H., Onda, Y., Hisadome, K., Loffredo, N., Kawamori, A., 2015. Temporal changes in radiocesium deposition in various forest stands following the Fukushima Dai-ichi Nuclear Power Plant accident. J. Environ. Radiact. http://dx.doi.org/10.1016/j.jenvrad.2015.04.016 (in press).

Leibundgut, C., Maloszewski, P., Külls, C., 2009. Tracers in Hydrology. John Wiley & Sons, Ltd, Chichester.

Loffredo, N., Onda, T., Kawamori, A., Kato, H., 2014. Modeling of leachable ^{137}Cs in throughfall and stemflow for Japanese forest canopies after Fukushima Daiichi nuclear power plant accident. Sci. Total Environ. 493, 701–707.

Mahara, Y., Ohta, T., Ogawa, H., Kumata, A., 2014. Atmospheric direct uptake and long-term fate of radiocesium in trees after the Fukushima nuclear accident. Sci. Rep. 4, 7121. http://dx.doi.org/10.1038/srep0721.

Ministry of Agriculture, Forestry and Fisheries (MAFF), 2014. The 88th Statistical

Yearbook of Ministry of Agriculture. Forestry and Fisheries (2012-2013). MAFF.
Ministry of Education, Culture, Sports, Science & Technology of Japan (MEXT), 2015. Extension Site of Distribution Map of Radiation Dose, etc.,/Digital Japan. http://ramap.jmc.or.jp/map/eng/ (accessed 17.03.15.).
Ministry of Land, Infrastructure, Transport and Tourism, 2015. Water Information System (In Japanese). http://www1.river.go.jp/ (accessed 19.03.15.).
Miura, S., Yoshinaga, S., Yamada, T., 2003. Protective effect of floor cover against soil erosion on steep slopes forested with *Chamaecyparis obtusa* (hinoki) and other species. J. For. Res. 8, 27–35.
National Astronomical Observatory of Japan, 2014. Chronological Scientific Tables 2013. Maruzen Publishing Co., Ltd., Tokyo.
Nishikiori, N., Ito, S., Tsuji, H., Yasutaka, T., Hayashi, S., 2015. Influence of forest floor covering on radiocesium wash-off associated with forest soil erosion. J. Jpn. For. Soc. 97, 63–69 (in Japanese with English abstract).
Ohnuki, T., Kozai, N., 2013. Adsorption behavior of radioactive cesium by non-mica minerals. J. Nucl. Sci. Technol. 50, 369–375.
Okada, N., Nakai, W., Ohashi, S., Tanaka, A., 2015. Radiocesium migration fro the canopy to the forest floor in pine and deciduous forests. J. Jpn. For. Soc. 97, 57–62 (in Japanese with English abstract).
Sawhney, B.L., 1970. Potassium and cesium ion selectivity in relation to clay mineral structure. Clay Clay Miner. 18, 47–52.
Schneider, C.A., Rasband, W.S., Eliceiri, K.W., 2012. NIH image to imageJ: 25 years of image analysis. Nat. Methods 9, 671–675.
Shaw, G., Belli, M., 1999. The RIFE models of radionuclide fluxed in European forest. In: Linkov, I., Schell, W.R. (Eds.), Contaminated Forest. Kluwer Academic Press, Netherlands, pp. 161–171.
Takahashi, J., Tamura, K., Suda, T., Matsumura, R., Onda, Y., 2015. Vertical distribution and temporal changes of ^{137}Cs in soil profiles under various land uses after the Fukushima Dai-ichi nuclear power plant accident. J. Environ. Radiact. 139, 351–361.
Tamura, T., Jacobs, D.G., 1960. Structural implication in cesium sorption. Health Phys. 2, 391–398.
Teramage, M.T., Onda, Y., Kato, H., Gomi, T., 2014. The role of litterfall in transferring Fukushima-derived radiocesium to a coniferous forest floor. Sci. Total Environ. 490, 435–439.
Tsukamoto, J., 1989. Movement of soil and litter down slopes in three types of forests (I) Movement of soil having particles less than two millimeters in diameter. J. Jpn. For. Soc. 71, 469–480 (in Japanese with English abstract).
Yoshimura, K., Onda, Y., Kato, H., 2015. Evaluation of radiocaesium wash-off by soil erosion from various land uses using USLE plots. J. Environ. Radiact. 139, 362–369.